Mechanism of C-Terminal Fragments of Amyloid β-Protein as Aβ Inhibitors: Do C-Terminal Interactions Play a Key Role in Their Inhibitory Activity?

Xueyun Zheng,[†] Chun Wu,[†,⊥] Deyu Liu,[†] Huiyuan Li,[‡] Gal Bitan,[‡,§] Joan-Emma Shea,[†,‖] and Michael T. Bowers*,[†]
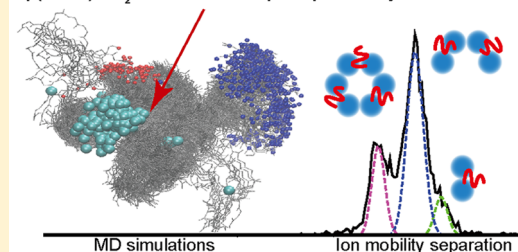
[†]Department of Chemistry and Biochemistry and [‖]Department of Physics, University of California, Santa Barbara, California 93106, United States

[‡]Department of Neurology, David Geffen School of Medicine, [§]Brain Research Institute, and Molecular Biology Institute, University of California at Los Angeles, Los Angeles, California 90095, United States

S *Supporting Information*

ABSTRACT: Targeting the early oligomerization of amyloid β protein (Aβ) is a promising therapeutic strategy for Alzheimer's disease (AD). Recently, certain C-terminal fragments (CTFs) derived from Aβ42 were shown to be potent inhibitors of Aβ-induced toxicity. The shortest peptide studied, Aβ(39−42), has been shown to modulate Aβ oligomerization and inhibit Aβ toxicity. Understanding the mechanism of these CTFs, especially Aβ(39−42), is of significance for future therapeutic development of AD and peptidomimetic-based drug development. Here we used ion mobility spectrometry−mass spectrometry to investigate the interactions between two modified Aβ(39−42) derivatives, VVIA-NH$_2$ and Ac-VVIA, and full-length Aβ42. VVIA-NH$_2$ was previously shown to

Aβ(39-42)-NH$_2$ interacts with Aβ42 specifically at C-terminus

MD simulations   Ion mobility separation

inhibit Aβ toxicity, whereas Ac-VVIA did not. Our mass spectrometry analysis revealed that VVIA-NH$_2$ binds directly to Aβ42 monomer and small oligomers while Ac-VVIA binds only to Aβ42 monomer. Ion mobility studies showed that VVIA-NH$_2$ modulates Aβ42 oligomerization by not only inhibiting the dodecamer formation but also disaggregating preformed Aβ42 dodecamer. Ac-VVIA also inhibits and removes preformed Aβ42 dodecamer. However, the Aβ42 sample with the addition of Ac-VVIA clogged the nanospray tip easily, indicating that larger aggregates are formed in the solution in the presence of Ac-VVIA. Molecular dynamics simulations suggested that VVIA-NH$_2$ binds specifically to the C-terminal region of Aβ42 while Ac-VVIA binds dispersedly to multiple regions of Aβ42. This work implies that C-terminal interactions and binding to Aβ oligomers are important for C-terminal fragment inhibitors.

■ INTRODUCTION

Amyloid β protein (Aβ) has been shown to play a significant role in the pathology of Alzheimer's disease (AD).[1] Aβ is produced from the amyloid precursor protein (APP) via proteolytic cleavages by β- and γ-secretases.[2] Aβ actually consists of a group of peptides containing 37−43 amino acid residues, among which Aβ40 and Aβ42 are the two primary alloforms (Aβ42 sequence: DAEFRHDSGY[10]-EVHHQKLVFF[20]AEDVGSNKGA[30]IIGLMVGGVV[40]IA). Although Aβ40 is more abundant than Aβ42 in vivo (Aβ40 constitutes ∼90% of all Aβ peptides), the latter is much more toxic and more aggregation prone. Recently an increased body of evidence has shown that the early oligomer states of Aβ, rather than the final fibrillar products, are the primary toxic agents in AD pathology.[3−6] In solution, Aβ42 forms dimers, tetramers, paranuclei (pentamers and hexamers), decamers and dodecamers, protofibrils, and eventually fibrils.[4,7,8] The 56 kDa dodecamer has been identified as a proximate toxic agent for AD pathology.[9,10] Therefore, targeting Aβ early oligomers, especially dodecamers, is a promising therapeutic strategy for AD treatment.

Short peptides derived from the Aβ sequence and their derivatives have been shown to disrupt Aβ assembly and inhibit its toxicity.[11,12] The C-terminal region of Aβ42, which is highly hydrophobic, has been shown to play an important role in controlling Aβ structure stability and self-assembly.[13−15] Thus, researchers hypothesized that peptides derived from the C-terminus of Aβ42 can serve as Aβ inhibitors, as they may interact with the C-terminal hydrophobic region of Aβ and be coassembled into Aβ42 oligomers, thereby disrupting their structures and inhibiting their toxicity.[16] Indeed, this C-terminal interaction hypothesis has led to the discovery of several effective C-terminal fragment (CTF) inhibitors of Aβ42

neurotoxicity, including peptides ranging from Aβ(29−42) to Aβ(39−42).[16]

Aβ(39−42), the shortest peptide studied, was shown to modulate Aβ oligomerization and inhibit Aβ neurotoxicity.[17−19] It is particularly interesting because it is a small molecule that can easily penetrate into membrane barriers. Thus, it is very important to understand the mechanism of its inhibitory activity for its future use in drug development and other peptidomimetics-based drug discovery. A previous theoretical study showed that Aβ(39−42) binds to several regions of Aβ42, including the N-terminal, central hydrophobic core, and C-terminal regions.[17] However, the key interaction region responsible for its inhibition activity remains unclear. To better understand the mechanism of action of Aβ(39−42), two terminally modified Aβ(39−42) analogues, N-terminal-acetylated Ac-VVIA and C-terminal-amidated VVIA-NH$_2$, were designed to test the effect of charge on the interactions between Aβ(39−42) and Aβ42. Previous studies have shown that modifications at the termini have very different effects on Aβ toxicity: VVIA-NH$_2$ inhibits Aβ-induced toxicity, while Ac-VVIA does not.[18]

Here, ion mobility spectrometry−mass spectrometry (IMS−MS) and all-atom molecular dynamics (MD) simulations were used to investigate the interactions between these two Aβ(39−42) analogues and full-length Aβ42. IMS is capable of separating species that have the same mass-to-charge ratio but different conformation or oligomer sizes.[20] It has been successfully applied in the past to study Aβ structure and assembly and the effects of small molecules.[8,17,21−29] In this work, we used IMS to examine the effects of these two Aβ(39−42) derivatives on the early assembly of Aβ42. MD simulations were performed to understand the details of the binding interactions between the Aβ42 and CTF molecules. This study provides an example of ion mobility spectrometry combined with theoretical modeling as a powerful tool to understand the mechanism of Aβ C-terminal fragments as small-molecule inhibitors of Aβ assembly and sheds light on the future use of a peptidomimetic-based therapeutic strategy for AD and other diseases.

■ EXPERIMENTAL PROCEDURES

Peptides and Sample Preparation. Full-length Aβ42 was synthesized by N-9-fluorenylmethoxycarbonyl (FMOC) chemistry.[30] Aβ(39−42) derivatives were prepared using a microwave-assisted peptide synthesizer as described previously.[18] The peptides were purified by reversed-phase HPLC, and their integrity was validated by mass spectrometry and amino acid analysis.

Ion Mobility Spectrometry−Mass Spectrometry. Lyophilized Aβ42 protein was dissolved in 10 mM ammonium acetate buffer (pH 7.4) with a final protein concentration of 10 μM. Mass spectra were recorded on a home-built nanoESI instrument, which has been described in detail elsewhere.[31] Briefly, ions are generated continuously by a nanoelectrospray ionization source, captured and guided through an ion funnel, injected into a temperature-controlled drift cell filled with 3−5 Torr helium gas, mass-analyzed with a quadrupole mass filter, and detected by a conversion dynode and channel electron multiplier, allowing a mass spectrum to be obtained.

For ion mobility measurements, the ions are stored in the ion funnel and pulsed into the drift cell. The injection energy of the ions can be varied from ∼20 to ∼150 V, but it is usually kept as low as possible to minimize thermal heating of the ions during the injection process. The ions gently pass through the cell under the influence of a weak electric field. The velocity of the ions in the drift cell, v_d, is proportional to the electric field E:

$$v_d = K \cdot E \tag{1}$$

Here, the proportionality constant K is termed the ion mobility. The ions exiting the drift cell are mass-selected and detected, allowing an arrival time distribution (ATD) to be recorded. The arrival time, t_A, is related to the time the ions spend in the drift cell, t_D, according to the expression $t_D = t_A - t_0$, where t_0 is the time between the ion's exit from the cell and arrival at the detector. The time in the cell is directly related to the ion mobility and collision cross section, $σ$, of the analyte ion as follows:[32]

$$\sigma = 1.3 \left(\frac{q^2 E^2 T}{\mu k_B p^2 N^2 l^2} \right)^{1/2} (t_A - t_0) \tag{2}$$

where q is the ion charge, E is the voltage across the drift cell, T is the absolute temperature, $μ$ is the reduced mass of the ion−He collision, k_B is the Boltzmann constant, p is the pressure, N is the buffer gas (helium) number density at STP, and l is the length of the drift cell (4.503 cm). All of these quantities are either known constants or are measured for each experiment. The width of the ATD can be compared with the width calculated for a single analyte ion structure,[33] which gives information on the distribution of oligomer structures in the ATD. The measured ion mobility and collision cross section provide information about the three-dimensional configurations of the ions.[8]

Transmission Electron Microscopy (TEM). Microscopic analysis was performed using an FEI T-20 transmission electron microscope operating at 200 kV. The Aβ42 samples were prepared using the same procedure as for mass spectrometry analysis. The samples were kept in a refrigerator (∼4 °C) for 2 weeks. For TEM measurements, 10 μL aliquots of the samples were spotted on glow-discharged carbon-coated copper grids (Ted Pella, Inc.). The samples on the grids were stained with 10 mM sodium metatungstate for 10 min and gently rinsed twice with deionized water. The sample grids were then dried at room temperature before TEM analysis.

Molecular Dynamics Simulations. *System Preparation.* Our simulation systems contained one Aβ42 peptide and one Aβ(39−42) derivative (VVIA-NH$_2$ or Ac-VVIA), ∼8000 water molecules, and several Na$^+$ ions to neutralize the system. The initial peptide structures of Aβ42 and Aβ(39−42) were taken from the previous study by Garcia and co-workers[13] and our previous study,[34] respectively. The Aβ(39−42) derivative was initially placed ∼15 Å away from the Aβ42 surface. The solute was immersed in a truncated octahedral box ($a = b = c ≈ 69$ Å, $α = β = γ = 109.47°$) filled with water molecules. The all-atom point-charge force field (AMBER ff03) of Duan et al.[35] was used to represent the peptides. This force field has been successfully used to model the binding of Aβ(39−42) to Aβ40/Aβ42 peptides,[17] binding among Aβ protofibrils,[36] and binding of fluorescent dyes to Aβ protofibrils.[37] The water solvent was explicitly represented by the TIP3P model.[38]

Binding Simulations. The AMBER 9 simulation suite[39] was used in the molecular dynamics simulations and data analysis. After an initial energy minimization, a total of eight simulations (four runs for each system) were performed with different initial random velocities. The random velocities of atoms were generated according to the Maxwell−Boltzmann distribution at
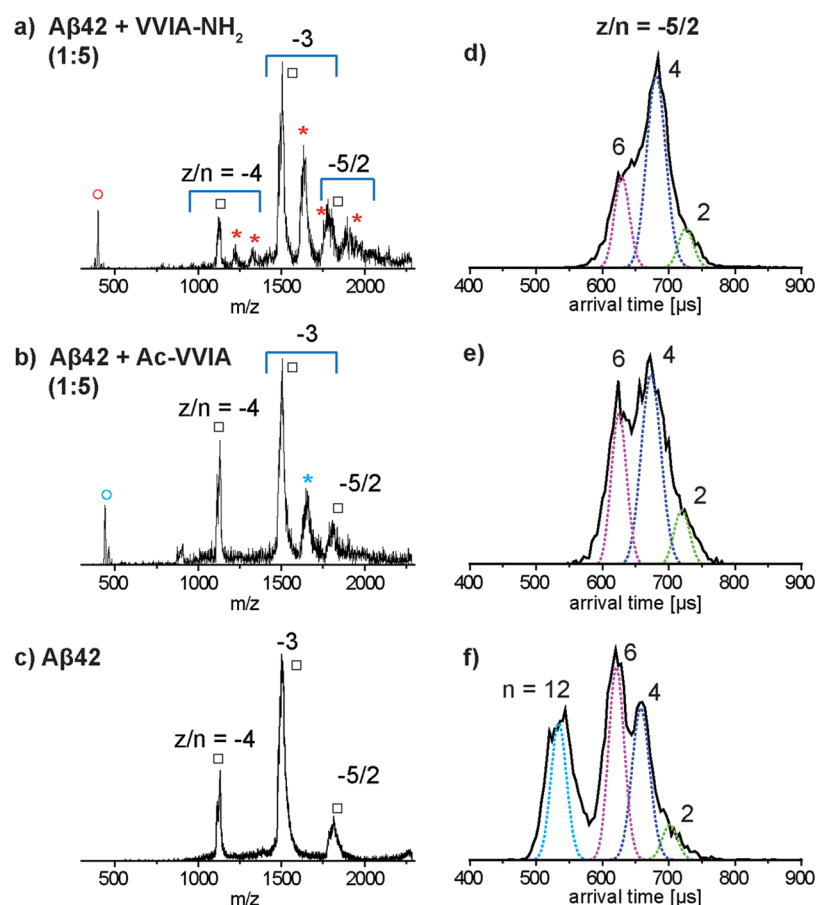
Figure 1. (a–c) Mass spectra of Aβ42 samples with and without CTF molecules. The charge states of each species are labeled with z/n, where z is the charge and n is the oligomer number. The Aβ42 peaks are denoted with open squares, the CTF molecule peaks with open circles, and the peaks for complexes of Aβ42 and CTF molecules with asterisks. (d–f) ATDs of the $z/n = -5/2$ peak for Aβ42 samples with and without CTF molecules. The oligomer number, n, is noted for each feature. The dashed lines represent the peak shapes expected for single structures in the ATD.

500 K. A 10 ps run at 500 K was used to further randomize the orientations and positions of the two peptides. The production run (150 ns) was conducted at 310 K and included a short (1 ns) period of MD in the *NPT* ensemble mode (constant pressure and temperature) to equilibrate the solvent and 149 ns of MD in the *NVT* ensemble mode (constant volume and temperature). Periodic boundary conditions were imposed on the system. The particle-mesh Ewald method[40] was used to treat the long-range electrostatic interactions. The SHAKE algorithm[41] was applied to constrain all of the bonds connecting hydrogen atoms, enabling the use of a 2 fs time step in the MD simulations. To reduce computation time, nonbonded forces were calculated using a two-stage RESPA approach[42] in which the short-range forces within a 10 Å radius were updated every step and the long-range forces beyond 10 Å were updated every two steps. Langevin dynamics was used to control the temperature at 310 K using a collision frequency of 1 ps^{-1}. The center of mass translation and rotation were removed every 500 steps, eliminating the "block of ice" problem.[43,44] The trajectories were saved at 10 ps intervals for analysis. In total, 128 Opteron CPU cores (2.3 GHz) were used for ∼50 days to complete the eight binding simulations (a cumulative MD time of 1.2 μs for the two systems).

Clustering Analysis. To gain a better understanding of the binding interactions, the stable complexes (>20 atom contacts) were grouped into different structural families on the basis of the Cα root mean square deviation (RMSD) of the complex

(cutoff of 5 Å) using the GROMACS protocol.[45] Representative structures (centroids) of the most abundant clusters from the combined four runs for each system are shown in Figures S2 and S3 in the Supporting Information.

Collision Cross Section Calculations. The centroids of the most abundant clusters were also used to calculate their collision cross sections by a projected superposition approximation (PSA) method.[46–49] To correlate better with the solvent-free experiments, these solution-phase structures were converted to "dehydrated" structures via a 500 000-step energy minimization in vacuum prior to cross-section calculations. This "dehydration" generally reduced the overall size of the structures while maintaining their solution structural features, and in this paper these structures are termed "dehydrated solution structures".

Binding Energy Calculations. The binding energy was evaluated on the centroid structure of a structural family using the molecular mechanics-generalized Born/surface area (MM-GBSA) module in the AMBER package. The solvation energy is represented by the generalized Born term (the polar part of the solvation) plus a surface area term (the hydrophobic part of the solvation free energy). Because the solute entropy is not included, the MM-GBSA binding energy tends to overestimate the absolute binding affinity. However, when the solute entropies in different binding modes are comparable, the relative binding affinities can be estimated from the relative MM-GBSA binding energies.[50]

■ RESULTS

Mass Spectrometry: VVIA-NH₂ Binds Directly to Aβ42 Monomer and Oligomers. The mass spectra of Aβ42 samples with and without VVIA analogues were recorded and are shown in Figure 1a−c. The mass spectrum of the Aβ42 sample without VVIA analogues (Figure 1c) shows three peaks corresponding to the $z/n = -4, -3$, and $-5/2$ charge states, where z is the charge and n is the oligomer number. In the mass spectrum of a 1:5 mixture of Aβ42 and VVIA-NH₂ (Figure 1a), there are more peaks in addition to the three Aβ42 peaks. These peaks correspond to $z/n = -4$ and -3 complexes of Aβ42 with one and two bound VVIA-NH₂ molecules (labeled with asterisks). Moreover, there is a peak tailing the $z/n = -5/2$ Aβ42 peak that corresponds to a $-5/2$ complex of Aβ42 oligomers with bound VVIA-NH₂ molecules. This indicates that VVIA-NH₂ binds directly not only to Aβ42 monomer but also to Aβ42 oligomers. The mass spectrum of a 1:5 mixture of Aβ42 and Ac-VVIA (Figure 1b) shows only one additional monomer complex peak, suggesting that only one Ac-VVIA binds directly to Aβ42 monomer. These results suggest that VVIA-NH₂ binds directly to Aβ42 with relatively higher affinity than Ac-VVIA. Unfortunately, Aβ42 aggregates so fast that we were not able to quantify this statement, but qualitatively, the higher intensity and greater number of adducts of VVIA-NH₂ relative to Ac-VVIA in mixtures with Aβ42 under identical conditions supports it.

Ion Mobility Studies: VVIA-NH₂ and Ac-VVIA Modulate the Early Assembly of Aβ42. To probe the effects of the two VVIA analogues on the early oligomer formation of Aβ42, an ion mobility study was performed, and the results are shown in Figure 1d−f. The ATD of the $-5/2$ peak for Aβ42 alone (Figure 1f) shows four features with arrival times of ∼710, 680, 610, and 540 μs, which were previously assigned as the Aβ42 dimer, tetramer, hexamer, and dodecamer, respectively, on the basis of their cross sections (see ref 8 for a detailed discussion of the $-5/2$ ATD assignment). The dodecamer was previously identified as a proximate toxic agent for AD pathology.[9,10] The ATD of the $-5/2$ peak for the Aβ42 sample with VVIA-NH₂ (1:5 ratio) shows only three features with arrival times of ∼720, 680, and 620 μs (Figure 1d), which can be assigned as the dimer, tetramer, and hexamer, respectively, on the basis of their cross sections. There are no features at shorter arrival times, indicating that no dodecamers or other larger oligomers formed in the presence of VVIA-NH₂. The ATD of the $-5/2$ peak for the Aβ42/Ac-VVIA mixture (1:5 ratio) shows three similar features corresponding to the dimer, tetramer, and hexamer (Figure 1e), suggesting that Ac-VVIA also inhibits the formation of Aβ42 dodecamer. However, the relative intensity of the hexamer in the presence of VVIA-NH₂ is lower than that in the presence of Ac-VVIA or Aβ42 alone, suggesting that VVIA-NH₂ not only inhibits dodecamer formation but also partially inhibits hexamer formation.

As shown in Figure 1a, an additional $z/n = -5/2$ oligomer complex peak was observed for the mixture of Aβ42 and VVIA-NH₂, and therefore, its ATD was also recorded to better understand the effect of VVIA-NH₂ on the Aβ42 oligomer distribution. The results are shown in Figure 2. The ATD shows three features with arrival times of ∼750, 710, and 640 μs, which can be assigned as the dimer, tetramer, and hexamer complexes, respectively, on the basis of their cross sections. This is of significance and suggests one, two, and three VVIA-NH₂ molecules are bound to Aβ42 dimer, tetramer, and
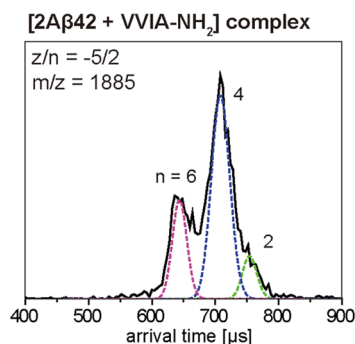

Figure 2. ATD of the $z/n = -5/2$ complex peak for the Aβ42 sample with VVIA-NH₂. The oligomer number, n, is noted for each feature.

hexamer, respectively, which is not observed for the sample with Ac-VVIA. The arrival times of tetramers and hexamers for adducts of Aβ42 with VVIA-NH₂ were $4 \pm 0.5\%$ longer than in pure Aβ42, which is about what would be expected from the percent increase in the number of residues in the adducts relative to neat Aβ42 (4.7%). Hence, no size difference is noted. This does not mean that there are not structural differences; it merely indicates that the cross sections do not dramatically change when VVIA-NH₂ is added to these oligomers.

Taken together, these mass spectrometry and ion mobility results suggest that both VVIA-NH₂ and Ac-VVIA bind to Aβ42 monomer and modulate dodecamer formation. However, VVIA-NH₂ binds not only to Aβ42 monomer but also to small Aβ42 oligomers (dimers, tetramers, and hexamers), while Ac-VVIA binds only to Aβ42 monomer. These results for VVIA-NH₂ are similar to previous results for VVIA, which binds to Aβ42 monomer and small oligomers and modulates dodecamer formation.[17] This is of significance since both VVIA and VVIA-NH₂ inhibit Aβ42-induced toxicity whereas Ac-VVIA does not.[17,18]

Disaggregation of Preformed Aβ42 Dodecamer by VVIA Analogues. To test whether these VVIA analogues can dissociate preformed Aβ42 oligomers, concentrated VVIA-NH₂ or Ac-VVIA was added to a preaggregated Aβ42 sample, and the ATDs of $z/n = -5/2$ Aβ42 were recorded at different time periods (Figure 3a−g). As shown in Figure 3a, after incubation for ∼5 h, wild-type Aβ42 forms dimers, tetramers, hexamers, and dodecamers. Immediately after the addition of VVIA-NH₂, the ATD of $z/n = -5/2$ Aβ42 shows only the three features corresponding to the dimer, tetramer, and hexamer but not the dodecamer feature (Figure 3b). The disappearance of the dodecamer peak suggests that VVIA-NH₂ can disassociate preformed dodecamers. The ATD of the $-5/2$ peak for the Aβ42 sample with added Ac-VVIA (Figure 3e) also shows only the dimer, tetramer, and hexamer features. However, the ATD of the Aβ42 sample with Ac-VVIA is noisier and broader than that for the VVIA-NH₂ sample, which suggests that there may be more families of oligomer structures for the Aβ42 sample with Ac-VVIA. This is important and consistent with the observation that it was more difficult to work with the Aβ42 sample with added Ac-VVIA: the sample with Ac-VVIA became difficult to spray, and the signal-to-noise ratio of the $z/n = -5/2$ ATD decreased over time (see Figure 3e−g). After 3 h, it became impossible to spray the sample with Ac-VVIA, and no further data could be collected. In contrast, the Aβ42 sample with added VVIA-NH₂ worked smoothly during the whole experiment time and even after several days (see Figure 3b−d). The ATD of the $-5/2$ peak recorded on the second day
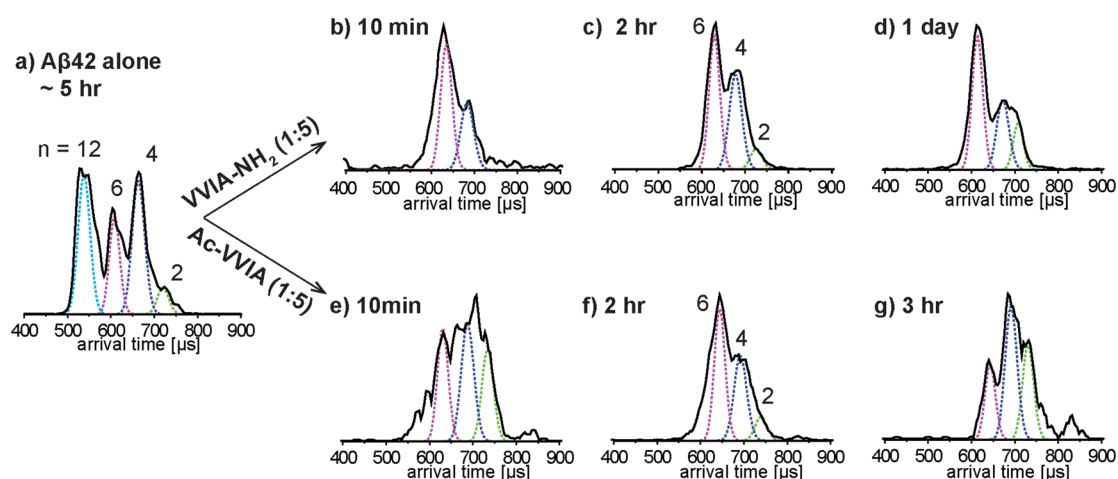
[2Aβ42 + VVIA-NH₂] complex

(Figure 2 inset labels: z/n = -5/2, m/z = 1885, n = 6, 4, 2, arrival time [μs], 400 500 600 700 800 900)

Figure 3. Time-dependent study of the dissociation of preformed Aβ42 oligomers by VVIA derivatives. (a) ATD of the $z/n = -5/2$ peak for an Aβ42 sample that was preincubated on ice for 5 h. (b–d) ATDs of the $z/n = -5/2$ peak for the Aβ42 sample after the addition of VVIA-NH$_2$ recorded after 10 min, 2 h, and 1 day. (e–g) ATDs of the $z/n = -5/2$ peak for the Aβ42 sample after the addition of Ac-VVIA recorded after 10 min, 2 h, and 3 h. The oligomer number, n, is noted for each feature in the ATDs. In (g), the peak at 840 μs is a noise peak.
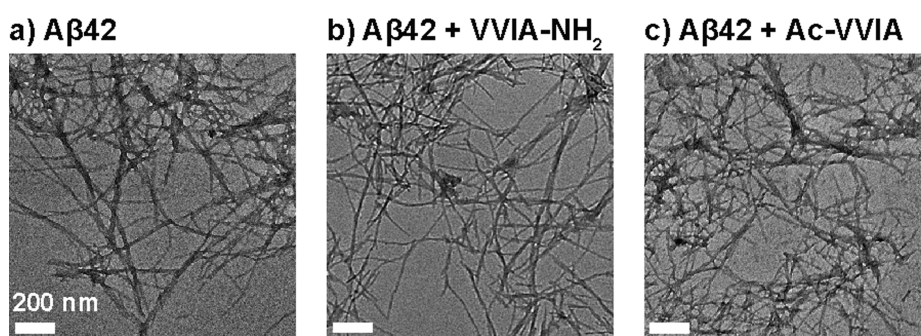

Figure 4. TEM images of Aβ42 samples incubated for 2 weeks without and with VVIA derivatives. Scale bars are 200 nm.
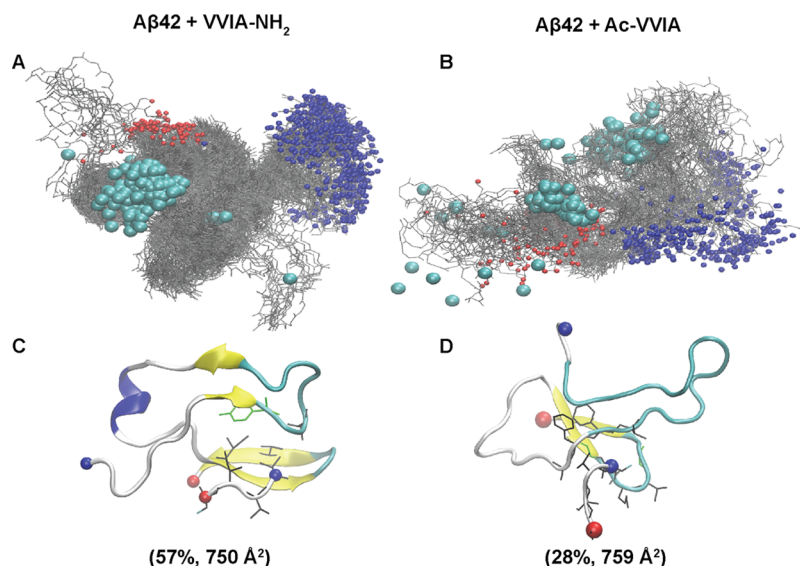

Figure 5. Interactions of Aβ42 with (A, C) VVIA-NH$_2$ and (B, D) Ac-VVIA. The N- and C-termini of Aβ42 are indicated by blue and red balls, respectively. (A, B) Superpositions of the complexes. The protein backbones are represented by the gray lines, and the VVIA derivatives are denoted by the larger cyan balls. (C, D) Representative bound complexes of the most populated structural families from the clustering analysis. The abundances and collision cross sections are noted. Only the side chains in contact with VVIA-NH$_2$/Ac-VVIA are shown (blue, positively charged; red, negatively charged; black, hydrophobic; green, hydrophilic). The 3-10-helical, β-extended, turn, and coiled conformations are colored in blue, yellow, cyan, and white, respectively.

(Figure 3d) still shows only the dimer, tetramer, and hexamer features. These results suggest that VVIA-NH$_2$ not only inhibits the formation of Aβ42 dodecamer but also dissociates preformed dodecamer. On the other hand, Ac-VVIA, which appears to inhibit dodecamer formation, may actually facilitate the formation of other larger oligomers or aggregates that clogged the spray tips. This qualitative observation of tip clogging suggests much faster formation of large aggregates for Ac-VVIA mixtures than for VVIA-NH$_2$ mixtures[21] and may well be the reason that Ac-VVIA does not reduce the toxicity of Aβ42 while VVIA-NH$_2$ does.

VVIA-NH$_2$ and Ac-VVIA Do Not Inhibit Aβ42 Fibril Formation. VVIA was previously shown to modulate Aβ42 oligomer formation but did not inhibit Aβ42 fibril formation. In this work, the effects of VVIA-NH$_2$ and Ac-VVIA on fibril formation were examined by TEM, and the results are shown in Figure 4. After incubation at 4 °C for 2 weeks, the Aβ42 samples formed abundant long fibrils regardless of the presence of VVIA-NH$_2$ or Ac-VVIA molecules. This suggests that neither VVIA-NH$_2$ nor Ac-VVIA inhibits Aβ42 fibril formation, which is similar to what was observed for VVIA.

Modeling the Interactions of Aβ42 with VVIA-NH$_2$ or Ac-VVIA. To probe the interactions of these two VVIA analogues with full-length Aβ42 at an atomic level, a system consisting of one Aβ42 and one VVIA-NH$_2$ or Ac-VVIA molecule was constructed for all-atom MD simulations. The most populated conformation of Aβ42 from the study of Sgourakis et al.[13] was used as the initial conformation in our simulations, enabling efficient sampling of the most important conformations.

The overall binding was revealed by superimposing the most stable complexes identified from the trajectories, as shown in Figure 5A,B. Aβ42 in both complexes shows great flexibility, as indicated by the widespread cloud of the overall peptide backbones (gray), which is expected as Aβ42 is a natively disordered peptide. However, the binding of VVIA-NH$_2$ to Aβ42 is more specific than that of Ac-VVIA. As shown in Figure 5A, the VVIA-NH$_2$ molecules bind exclusively to only one specific region of Aβ42, the hydrophobic C-terminal region. The representative structure of the most populated structural family (57% of the total population) from our clustering analysis shows that VVIA-NH$_2$ binds to the edge of the C-terminal β-hairpin (Figure 5C). On the other hand, Ac-VVIA molecules are observed to bind to several regions of Aβ42, including the C-terminal, central hydrophobic core, and N-terminal regions (Figures 5B and S3). Clearly, the binding of Ac-VVIA to Aβ42 is more disperse, and the most populated structural family only contains 28% of the total population (Figure 5D). Moreover, the Aβ42:VVIA-NH$_2$ complexes appear to be more rigid and display a uniform conformation, whereas the Aβ42:Ac-VVIA complexes show more flexible and extended structures with slightly larger collision cross sections.

VVIA was previously shown to bind to Aβ42 in several regions, including the C-terminal, central hydrophobic core, and N-terminal regions.[17] The binding simulations of VVIA derivatives presented here reveal significant differences in their binding interactions with Aβ42. While the binding of Ac-VVIA to the C-terminal part of Aβ42 is slightly reduced in comparison with that of VVIA,[17] the binding of VVIA-NH$_2$ to the C-terminal part of Aβ42 is significantly increased. Electrostatic interactions contribute to these changes, as the negatively charged C-terminus of Ac-VVIA repels the negatively charged C-terminus of Aβ42 while the positively charged N-

terminus of VVIA-NH$_2$ is attracted to the negatively charged C-terminus of Aβ42. This attraction is manifested in a strong binding energy of −105 kcal/mol for Aβ42 with VVIA-NH$_2$, which is dramatically larger than the computed binding energy of −20 kcal/mol with Ac-VVIA (the binding energy for each representative structure of the complexes is noted in Figures S2 and S3). The correlation between the ability of VVIA-NH$_2$ to inhibit Aβ42 oligomerization and toxicity and the binding of this peptide specifically to the C-terminal hydrophobic region of Aβ42 implies an important role of the C-terminal region in the structural stability, assembly, and toxicity of Aβ42 and its inhibition by C-terminal fragments.

Aβ42 Monomer Complexes. The ATDs of the $z/n = -3$ Aβ42 monomer and its complexes with the VVIA analogues were recorded, and the results are shown in Figures S4 and S5 and Table S1. The ATDs of the $z/n = -3$ monomer and its complexes with one VVIA analogue are shown in Figure 6. The
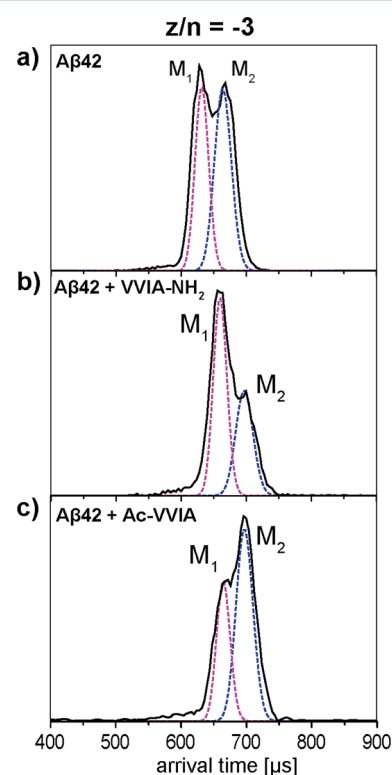

Figure 6. ATDs of (a) the $z/n = -3$ monomer and (b) its complexes with (b) VVIA-NH$_2$ and (c) Ac-VVIA. M$_1$ and M$_2$ represent the two monomer conformers of Aβ42.

ATD of the Aβ42 monomer shows two features that were previously assigned as a gas-phase-like compact conformer, M$_1$, and a solution-like conformer, M$_2$ (Figure 6a).[51] The ATDs of the complexes of Aβ42 monomer with one VVIA-NH$_2$ or Ac-VVIA show two similar features (Figure 6b,c). By analogy, they can be assigned as a gas-phase-like conformer and a solution-like conformer. The cross sections were measured and showed size increases of ∼5−6% after the addition of one VVIA analogue (Table 1), which is probably due to the addition of the four residues of the CTFs. The experimental cross section for the solution-like structure is similar to the theoretical values for the most populated structure (Table 1).

Table 1. Experimental and Theoretical Cross Sections, σ, for the $z/n = -3$ Aβ42 Monomer and Its Complexes

species	Aβ42		with one VVIA-NH$_2$		with one Ac-VVIA	
	M$_1$	M$_2$	M$_1$	M$_2$	M$_1$	M$_2$
σ_{exptl} (Å^2)^a	631	707	668	748	670	742
σ_{PSA} (Å^2)				750		759

^{a}The errors in the experimental cross sections are $\leq$1%.

■ DISCUSSION AND CONCLUSIONS

A previous study showed that VVIA-NH$_2$ inhibits Aβ toxicity while Ac-VVIA does not.[18] Our mass spectrometry and ion mobility studies have revealed that VVIA-NH$_2$ and Ac-VVIA have different effects on Aβ42 early assembly. VVIA-NH$_2$ binds directly not only to Aβ42 monomer (binding of up to two VVIA-NH$_2$ molecules to Aβ42 monomer was observed) but also to small Aβ42 oligomers (dimers, tetramers, and hexamers). Importantly, VVIA-NH$_2$ also inhibits dodecamer formation and removes preformed dodecamers. On the other hand, only binding of one Ac-VVIA molecule directly to Aβ42 monomer was observed. Ac-VVIA also appears to modulate dodecamer formation. However, the Aβ42 sample with added Ac-VVIA showed broader ATDs, indicating more complicated structures and oligomer distributions, and the sample clogged the nanospray tip easily. The nanoESI system completely stopped working after incubation for 3 h, indicating that large aggregates formed in the solution, likely through pathways that bypass dodecamer formation. These differences reflect the different binding of VVIA-NH$_2$ and Ac-VVIA to Aβ42 and are consistent with their different abilities to inhibit Aβ42 toxicity. A summary of the differences among the assembly modes for the various systems is given in Figure 7. It is worth noting that uncapped VVIA reacts similarly to VVIA-NH$_2$ in that they both bind to Aβ42 monomer and oligomers and both strongly

Figure 7. Aggregation mechanism of Aβ42 in the absence or presence of VVIA-NH$_2$ or Ac-VVIA. VVIA-NH$_2$ binds directly to Aβ42 monomer and small oligomers (dimers, tetramers, and hexamers), inhibiting the formation of dodecamers and driving the formation of nontoxic oligomers that eventually form fibrils. Ac-VVIA binds only to Aβ42 monomer, inhibiting the formation of the dodecamer. However, Ac-VVIA binding may lead to other pathways bypassing the dodecamer and forming other toxic oligomers or aggregates, which eventually form fibrils.

reduce the toxicity of Aβ42.[17] Hence, it appears important for the CTF to bind not only to Aβ42 monomer but also to the small oligomers to be effective.

Our MD binding simulations have shown significantly different binding interactions of VVIA-NH$_2$ and Ac-VVIA with Aβ42. Ac-VVIA binds in a dispersed fashion to Aβ42 at multiple sites, including the C-terminal, central, and N-terminal regions. In contrast, VVIA-NH$_2$, the effective Aβ42 inhibitor, binds specifically to only the C-terminal β-hairpin region of Aβ42. This is of significance and implies that interactions with the C-terminal region, rather than with other regions, may be the key for the inhibition activity of Aβ(39−42).

The C-terminal hydrophobic region of Aβ42 has been considered to play an important role in the structural stability and assembly of Aβ42.[7,52] A recent study of Aβ42 fibrils showed that the C-terminal Ala42, which is absent in Aβ40, forms a unique salt bridge with Lys28 to create an Aβ42-selective self-recognizing and self-replicating amyloid propagation machinery in AD pathology.[53] Moreover, previous studies of prefibrillar Aβ42 showed that the Ile41 and Ala42 residues stabilize the C-terminal turn conformation causing Aβ42 to have a more rigid C-terminus than Aβ40.[13] The increased conformational stability of the C-terminus is correlated with the formation of more toxic oligomers in Aβ42, which explains how the difference of only two residues between Aβ40 and Aβ42 can significantly change the toxicity and aggregation properties of Aβ proteins.[13] These C-terminal hydrophobic residues in Aβ42 have been considered to be the driving force for protein folding and self-assembly and to stabilize neurotoxic low-order oligomers.[14] Therefore, the hypothesis that peptides derived from the C-terminus of Aβ42 may be coassembled into Aβ42 monomer and oligomers and disrupt their structures, thereby inhibiting their toxicity, led to the successful discovery of effective C-terminal fragment inhibitors.[16] However, recent studies using intrinsic tyrosine fluorescence and NMR methods suggested that Aβ(39−42) might primarily interact with the N-terminus of Aβ42.[18] Our earlier simulations of the binding of Aβ(39−42) to Aβ42 corroborated this picture, as Aβ(39−42) was observed to bind to multiple sites of Aβ42. These regions included the C-terminal, central hydrophobic core, and N-terminal regions.[17] These studies were intriguing because they did not seem to be in line with the original hypothesis that the C-terminal peptide inhibitors would specifically target the C-terminus of Aβ42. The peptide inhibitor VVIA-NH$_2$ binds specifically to the C-terminus of Aβ42 monomers and oligomers, resulting in effective inhibition of Aβ42 toxicity. However, VVIA is also an effective inhibitor of toxicity and an indiscriminate binder to Aβ42, so C-terminal binding cannot be the exclusive determining factor. What VVIA and VVIA-NH$_2$ have in common is strong binding to both monomers and oligomers of Aβ42, whereas Ac-VVIA binds more weakly to Aβ42 monomer and not at all to its oligomers. Thus, binding to Aβ42 oligomers appears to be crucial for the inhibition of toxicity, but more research is needed to fully understand the mechanism at play.
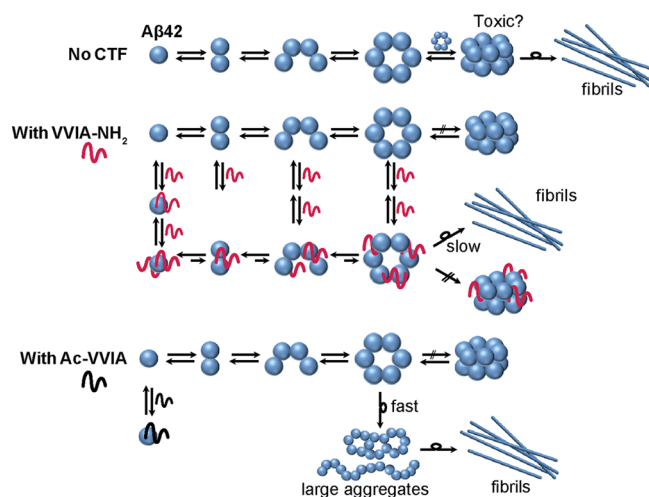
■ ASSOCIATED CONTENT

Ⓢ Supporting Information

The Supporting Information is available free of charge on the ACS Publications website at DOI: 10.1021/acs.jpcb.5b08177.

Additional information on starting structures of Aβ42 and VVIA analogues for MD simulations, structures of

representative complexes of Aβ42 with VVIA analogues from MD simulations, and ATDs and cross sections of Aβ42 monomer and monomer complexes (PDF)

■ AUTHOR INFORMATION

Corresponding Author

*E-mail: bowers@chem.ucsb.edu. Telephone: 805-893-2893. Fax: 805-893-8703.

Present Address

$^{\perp}$C.W.: Department of Chemistry and Biochemistry and Department of Biomedical and Translational Sciences, Rowan University, Glassboro, New Jersey 08028, United States.

Notes

The authors declare no competing financial interest.

■ REFERENCES

(1) Mattson, M. P. Pathways Towards and Away from Alzheimer's Disease. *Nature* **2004**, *430*, 631–639.

(2) O'Brien, R. J.; Wong, P. C. Amyloid Precursor Protein Processing and Alzheimer's Disease. *Annu. Rev. Neurosci.* **2011**, *34*, 185–204.

(3) Teplow, D. On the Subject of Rigor in the Study of Amyloid β-Protein Assembly. *Alzheimer's Res. Ther.* **2013**, *5*, 39.

(4) Teplow, D. B.; Lazo, N. D.; Bitan, G.; Bernstein, S.; Wyttenbach, T.; Bowers, M. T.; Baumketner, A.; Shea, J. E.; Urbanc, B.; Cruz, L.; et al. Elucidating Amyloid β-Protein Folding and Assembly: A Multidisciplinary Approach. *Acc. Chem. Res.* **2006**, *39*, 635–645.

(5) Walsh, D. M.; Selkoe, D. J. Aβ Oligomers - A Decade of Discovery. *J. Neurochem.* **2007**, *101*, 1172–1184.

(6) Hayden, E.; Teplow, D. Amyloid β-Protein Oligomers and Alzheimer's Disease. *Alzheimer's Res. Ther.* **2013**, *5*, 60.

(7) Bitan, G.; Kirkitadze, M. D.; Lomakin, A.; Vollers, S. S.; Benedek, G. B.; Teplow, D. B. Amyloid β-Protein (Aβ) Assembly: Aβ40 And Aβ42 Oligomerize through Distinct Pathways. *Proc. Natl. Acad. Sci. U. S. A.* **2003**, *100*, 330–335.

(8) Bernstein, S. L.; Dupuis, N. F.; Lazo, N. D.; Wyttenbach, T.; Condron, M. M.; Bitan, G.; Teplow, D. B.; Shea, J.-E.; Ruotolo, B. T.; Robinson, C. V.; et al. Amyloid-β Protein Oligomerization and the Importance of Tetramers and Dodecamers in the Aetiology of Alzheimer's Disease. *Nat. Chem.* **2009**, *1*, 326–331.

(9) Gong, Y.; Chang, L.; Viola, K. L.; Lacor, P. N.; Lambert, M. P.; Finch, C. E.; Krafft, G. A.; Klein, W. L. Alzheimer's Disease-Affected Brain: Presence of Oligomeric Aβ Ligands (ADDLs) Suggests a Molecular Basis for Reversible Memory Loss. *Proc. Natl. Acad. Sci. U. S. A.* **2003**, *100*, 10417–10422.

(10) Lesné, S.; Koh, M. T.; Kotilinek, L.; Kayed, R.; Glabe, C. G.; Yang, A.; Gallagher, M.; Ashe, K. H. A Specific Amyloid-β Protein Assembly in the Brain Impairs Memory. *Nature* **2006**, *440*, 352–357.

(11) Tjernberg, L. O.; Näslund, J.; Lindqvist, F.; Johansson, J.; Karlström, A. R.; Thyberg, J.; Terenius, L.; Nordstedt, C. Arrest of β-Amyloid Fibril Formation by a Pentapeptide Ligand. *J. Biol. Chem.* **1996**, *271*, 8545–8548.

(12) Arai, T.; Sasaki, D.; Araya, T.; Sato, T.; Sohma, Y.; Kanai, M. A Cyclic KLVFF-Derived Peptide Aggregation Inhibitor Induces the Formation of Less-Toxic Off-Pathway Amyloid-β Oligomers. *ChemBioChem* **2014**, *15*, 2577–2583.

(13) Sgourakis, N. G.; Yan, Y.; McCallum, S. A.; Wang, C.; Garcia, A. E. The Alzheimer's Peptides Aβ40 and 42 Adopt Distinct Conformations in Water: A Combined MD/NMR Study. *J. Mol. Biol.* **2007**, *368*, 1448–1457.

(14) Ahmed, M.; Davis, J.; Aucoin, D.; Sato, T.; Ahuja, S.; Aimoto, S.; Elliott, J. I.; Van Nostrand, W. E.; Smith, S. O. Structural Conversion of Neurotoxic Amyloid-β_{1-42} Oligomers to Fibrils. *Nat. Struct. Mol. Biol.* **2010**, *17*, 561–567.

(15) Wei, G.; Jewett, A. I.; Shea, J.-E. Structural Diversity of Dimers of the Alzheimer Amyloid-β(25–35) Peptide and Polymorphism of the Resulting Fibrils. *Phys. Chem. Chem. Phys.* **2010**, *12*, 3622–3629.

(16) Fradinger, E. A.; Monien, B. H.; Urbanc, B.; Lomakin, A.; Tan, M.; Li, H.; Spring, S. M.; Condron, M. M.; Cruz, L.; Xie, C.-W.; et al. C-Terminal Peptides Coassemble into Aβ42 Oligomers and Protect Neurons against Aβ42-Induced Neurotoxicity. *Proc. Natl. Acad. Sci. U. S. A.* **2008**, *105*, 14175–14180.

(17) Gessel, M. M.; Wu, C.; Li, H.; Bitan, G.; Shea, J.-E.; Bowers, M. T. Aβ(39–42) Modulates Aβ Oligomerization but Not Fibril Formation. *Biochemistry* **2012**, *51*, 108–117.

(18) Li, H.; Du, Z.; Lopes, D. H. J.; Fradinger, E. A.; Wang, C.; Bitan, G. C-Terminal Tetrapeptides Inhibit Aβ42-Induced Neurotoxicity Primarily through Specific Interaction at the N-Terminus of Aβ42. *J. Med. Chem.* **2011**, *54*, 8451–8460.

(19) Li, H.; Monien, B. H.; Lomakin, A.; Zemel, R.; Fradinger, E. A.; Tan, M.; Spring, S. M.; Urbanc, B.; Xie, C.-W.; Benedek, G. B.; et al. Mechanistic Investigation of the Inhibition of Aβ42 Assembly and Neurotoxicity by Aβ42 C-Terminal Fragments. *Biochemistry* **2010**, *49*, 6358–6364.

(20) Wyttenbach, T.; Bowers, M. T. Gas-Phase Conformations: The Ion Mobility/Ion Chromatography Method. *Top. Curr. Chem.* **2003**, *225*, 207–232.

(21) Bernstein, S. L.; Wyttenbach, T.; Baumketner, A.; Shea, J.-E.; Bitan, G.; Teplow, D. B.; Bowers, M. T. Amyloid β-protein: Monomer Structure and Early Aggregation States of Aβ42 and Its Pro19 Alloform. *J. Am. Chem. Soc.* **2005**, *127*, 2075–2084.

(22) Bleiholder, C.; Dupuis, N. F.; Wyttenbach, T.; Bowers, M. T. Ion Mobility-Mass Spectrometry Reveals a Conformational Conversion from Random Assembly to β-Sheet in Amyloid Fibril Formation. *Nat. Chem.* **2011**, *3*, 172–177.

(23) Gessel, M. M.; Bernstein, S.; Kemper, M.; Teplow, D. B.; Bowers, M. T. Familial Alzheimer's Disease Mutations Differentially Alter Amyloid β-Protein Oligomerization. *ACS Chem. Neurosci.* **2012**, *3*, 909–918.

(24) Zheng, X.; Liu, D.; Roychaudhuri, R.; Teplow, D. B.; Bowers, M. T. Amyloid β-Protein Assembly: Differential Effects of the Protective A2T Mutation and Recessive A2V Familial Alzheimer's Disease Mutation. *ACS Chem. Neurosci.* **2015**, DOI: 10.1021/acschemneuro.5b00171.

(25) Lee, S.; Zheng, X.; Krishnamoorthy, J.; Savelieff, M. G.; Park, H. M.; Brender, J. R.; Kim, J. H.; Derrick, J. S.; Kochi, A.; Lee, H. J.; et al. Rational Design of a Structural Framework with Potential Use to Develop Chemical Reagents That Target and Modulate Multiple Facets of Alzheimer's Disease. *J. Am. Chem. Soc.* **2014**, *136*, 299–310.

(26) Zheng, X.; Gessel, M. M.; Wisniewski, M. L.; Viswanathan, K.; Wright, D. L.; Bahr, B. A.; Bowers, M. T. Z-Phe-Ala-diazomethylketone (PADK) Disrupts and Remodels Early Oligomer States of the Alzheimer Disease Aβ42 Protein. *J. Biol. Chem.* **2012**, *287*, 6084−6088.

(27) Zheng, X.; Liu, D.; Klärner, F.-G.; Schrader, T.; Bitan, G.; Bowers, M. T. Amyloid β-Protein Assembly: The Effect of Molecular Tweezers CLR01 and CLR03. *J. Phys. Chem. B* **2015**, *119*, 4831−4841.

(28) Soper, M. T.; DeToma, A. S.; Hyung, S.-J.; Lim, M. H.; Ruotolo, B. T. Amyloid-β-Neuropeptide Interactions Assessed by Ion Mobility-Mass Spectrometry. *Phys. Chem. Chem. Phys.* **2013**, *15*, 8952−8961.

(29) Young, L. M.; Saunders, J. C.; Mahood, R. A.; Revill, C. H.; Foster, R. J.; Tu, L. H.; Raleigh, D. P.; Radford, S. E.; Ashcroft, A. E. Screening and Classifying Small-Molecule Inhibitors of Amyloid Formation Using Ion Mobility Spectrometry-Mass Spectrometry. *Nat. Chem.* **2015**, *7*, 73−81.

(30) Lomakin, A.; Chung, D. S.; Benedek, G. B.; Kirschner, D. A.; Teplow, D. B. On the Nucleation and Growth Of Amyloid β-Protein Fibrils: Detection of Nuclei and Quantitation of Rate Constants. *Proc. Natl. Acad. Sci. U. S. A.* **1996**, *93*, 1125−1129.

(31) Wyttenbach, T.; Kemper, P. R.; Bowers, M. T. Design of a New Electrospray Ion Mobility Mass Spectrometer. *Int. J. Mass Spectrom.* **2001**, *212*, 13−23.

(32) Gidden, J.; Ferzoco, A.; Baker, E. S.; Bowers, M. T. Duplex Formation and the Onset of Helicity in Poly d(CG)n Oligonucleotides in a Solvent-Free Environment. *J. Am. Chem. Soc.* **2004**, *126*, 15132−15140.

(33) Mason, E. A.; McDaniel, E. W. Kinetic Theory of Mobility and Diffusion. In *Transport Properties of Ions in Gases*; Wiley-VCH: Weinheim, Germany, 2005; Sections 5.1−5.2, pp 137−193.

(34) Wu, C.; Murray, M. M.; Bernstein, S. L.; Condron, M. M.; Bitan, G.; Shea, J. E.; Bowers, M. T. The Structure of Aβ42 C-Terminal Fragments Probed by a Combined Experimental and Theoretical Study. *J. Mol. Biol.* **2009**, *387*, 492−501.

(35) Duan, Y.; Chowdhury, S.; Xiong, G.; Wu, C.; Zhang, W.; Lee, T.; Cieplak, P.; Caldwell, J.; Luo, R.; Wang, J.; et al. A Point-Charge Force Field for Molecular Mechanics Simulations of Proteins Based on Condensed-Phase QM Calculations. *J. Comput. Chem.* **2003**, *24*, 1999−2012.

(36) Wu, C.; Bowers, M. T.; Shea, J. E. Molecular Structures of Quiescently Grown and Brain-Derived Polymorphic Fibrils of the Alzheimer Amyloid Aβ$_{9−40}$ Peptide: A Comparison to Agitated Fibrils. *PLoS Comput. Biol.* **2010**, *6*, e1000693.

(37) Wu, C.; Wang, Z. X.; Lei, H. X.; Zhang, W.; Duan, Y. Dual Binding Modes of Congo Red to Amyloid Protofibril Surface Observed in Molecular Dynamics Simulations. *J. Am. Chem. Soc.* **2007**, *129*, 1225−1232.

(38) Jorgensen, W. L.; Chandrasekhar, J.; Madura, J. D.; Impey, R. W.; Klein, M. L. Comparisons of Simple Potential Functions for Simulating Liquid Water. *J. Chem. Phys.* **1983**, *79*, 926−935.

(39) Wang, J. M.; Wolf, R. M.; Caldwell, J. W.; Kollman, P. A.; Case, D. A. Development and Testing of a General Amber Force Field. *J. Comput. Chem.* **2004**, *25*, 1157−1174.

(40) Essmann, U.; Perera, L.; Berkowitz, M. L.; Darden, T. A.; Lee, H.; Pedersen, L. G. A Smooth Particle Mesh Ewald Method. *J. Chem. Phys.* **1995**, *103*, 8577−8593.

(41) Ryckaert, J.-P.; Ciccotti, G.; Berendsen, H. J. C. Numerical Integration of the Cartesian Equations of Motion of a System with Constraints: Molecular Dynamics of N-Alkanes. *J. Comput. Phys.* **1977**, *23*, 327−341.

(42) Procacci, P.; Berne, B. J. Multiple Time-Scale Methods for Constant-Pressure Molecular-Dynamics Simulations of Molecular-Systems. *Mol. Phys.* **1994**, *83*, 255−272.

(43) Chiu, S. W.; Clark, M.; Subramaniam, S.; Jakobsson, E. Collective Motion Artifacts Arising in Long-Duration Molecular Dynamics Simulations. *J. Comput. Chem.* **2000**, *21*, 121−131.

(44) Harvey, S. C.; Tan, R. K. Z.; Cheatham, T. E. The Flying Ice Cube: Velocity Rescaling in Molecular Dynamics Leads to Violation of Energy Equipartition. *J. Comput. Chem.* **1998**, *19*, 726−740.

(45) Daura, X.; Gademann, K.; Jaun, B.; Seebach, D.; van Gunsteren, W. F.; Mark, A. E. Peptide Folding: When Simulation Meets Experiment. *Angew. Chem., Int. Ed.* **1999**, *38*, 236−240.

(46) Bleiholder, C.; Wyttenbach, T.; Bowers, M. T. A Novel Projection Approximation Algorithm for the Fast and Accurate Computation of Molecular Collision Cross Sections (I). Method. *Int. J. Mass Spectrom.* **2011**, *308*, 1−10.

(47) Bleiholder, C.; Contreras, S.; Do, T. D.; Bowers, M. T. A Novel Projection Approximation Algorithm for the Fast and Accurate Computation of Molecular Collision Cross Sections (II). Model Parameterization and Definition of Empirical Shape Factors for Proteins. *Int. J. Mass Spectrom.* **2013**, *345−347*, 89−96.

(48) Anderson, S. E.; Bleiholder, C.; Brocker, E. R.; Stang, P. J.; Bowers, M. T. A Novel Projection Approximation Algorithm for the Fast and Accurate Computation of Molecular Collision Cross Sections (III): Application to Supramolecular Coordination-Driven Assemblies with Complex Shapes. *Int. J. Mass Spectrom.* **2012**, *330−332*, 78−84.

(49) Bleiholder, C.; Contreras, S.; Bowers, M. T. A Novel Projection Approximation Algorithm for the Fast and Accurate Computation of Molecular Collision Cross Sections (IV). Application to Polypeptides. *Int. J. Mass Spectrom.* **2013**, *354−355*, 275−280.

(50) Kongsted, J.; Soderhjelm, P.; Ryde, U. How Accurate Are Continuum Solvation Models for Drug-Like Molecules? *J. Comput.-Aided Mol. Des.* **2009**, *23*, 395−409.

(51) Baumketner, A.; Bernstein, S. L.; Wyttenbach, T.; Bitan, G.; Teplow, D. B.; Bowers, M. T.; Shea, J.-E. Amyloid β-Protein Monomer Structure: A Computational and Experimental Study. *Protein Sci.* **2006**, *15*, 420−428.

(52) Lazo, N. D.; Grant, M. A.; Condron, M. C.; Rigby, A. C.; Teplow, D. B. On the Nucleation of Amyloid β-Protein Monomer Folding. *Protein Sci.* **2005**, *14*, 1581−1596.

(53) Xiao, Y.; Ma, B.; McElheny, D.; Parthasarathy, S.; Long, F.; Hoshi, M.; Nussinov, R.; Ishii, Y. Aβ(1−42) Fibril Structure Illuminates Self-Recognition and Replication of Amyloid in Alzheimer's Disease. *Nat. Struct. Mol. Biol.* **2015**, *22*, 499−505.